Dependence of Atmospheric Cooling by Vegetation on Canopy Surface Area During Radiative Cooling at Night: Physical Model Evaluation Using a Polyethylene Chamber

Maki OKADA [a, †], Masumi OKADA [b] and Hiroyuki KUSAKA [a]

（
[a] Center for Computational Sciences, University of Tsukuba, 1−1−1 Tennodai, Tsukuba, Ibaraki 305−8577, Japan
[b] Faculty of Agriculture, Iwate University, 3−18−8 Ueda, Morioka, Iwate 020−8550, Japan
）

Abstract

The plant canopy surface is cooled by radiative cooling at night. Cooling of the canopy surface results in cooling of the surrounding air by convective heat exchange between the canopy surface and the air. Convective heat exchange at the canopy surface is proportional to the convective heat transfer conductance, which depends on the wind speed and the canopy surface area. We conducted physical model experiments using a polyethylene chamber to examine the dependence of the heat exchange at the canopy surface on the canopy surface area during nocturnal radiative cooling. We introduced three canopy models, each having a canopy surface area equivalent to a Leaf Area Index （LAI） of 1, 2, or 4. The models were placed in two polyethylene chambers located outdoors and exposed to a nocturnal radiation regime. The canopy surface temperature of the LAI = 1 model was the lowest among the three models, whereas the convective heat exchange between the canopy surface and the air traveling into the chamber was the smallest for the LAI = 1 model. The convective heat exchange did not differ significantly between the LAI = 2 and 4 canopy models. The results showed that the air traveling through the canopy was cooled more at night, when the canopy LAI was large and the canopy surface temperature was relatively high. This air-cooling effect tended to approach an asymptotic value as the LAI became large. We were able to simulate these phenomena with a simple heat balance analysis of the heat exchange between the canopy surface and the air.

Key words: Canopy surface area, Heat balance, Heat exchange, Physical model experiment, Polyethylene chamber.

1. Introduction

A plant canopy is effective at cooling surrounding air by transpiration in the daytime and by radiative cooling at night. Because this air-cooling effect is expected to mitigate heat discomfort in an urban area, many studies have investigated the effects of an urban green park or roadside trees on the thermal environment of adjacent built-up areas. Although the relative coolness of these green areas has been well known, there is incomplete understanding of the roles of canopy cover in the processes of air-cooling, and in particular of the roles associated with radiative cooling at night. Hence there is still debate about what type of vegetation is most effective in cooling air.

Previous studies （Kanda and Hino, 1990a,b; Honjo and Takakura, 2000a,b; Huang *et al.*, 2011） have used numerical simulation approaches to compare an aggregated plant canopy to a sparsely scattered plant canopy and have concluded that a scattered plant canopy is more effective in cooling the surrounding urban atmosphere. It is not surprising that a scattered canopy is more effective than an aggregated canopy in exchanging heat convectively between the cooled canopy surface and the surrounding air. Although these studies dealt with heat exchange processes in the daytime, their conclusions may be true for a plant canopy cooled radiatively at night; namely, the enhancement of air-cooling is greater when the convective heat exchange at the canopy surface is larger.

Assuming steady state conditions and no latent heat transfer, heat gain by convection from the air and heat loss by radiation are balanced at the canopy surface. At night, a larger heat exchange due to convection leads to an increase of canopy surface temperature as well as to an increase of the rate of radiative dissipation of heat to the sky and/or surrounding surfaces because of the higher surface temperature of the canopy. Surfaces with higher temperature lose more heat through radiation; they therefore gain more heat from the air and consequently cool the surrounding air more efficiently. Okada *et al.* （2014） have experimentally demonstrated this mechanism with a physical model using a polyethylene （PE） chamber; namely, air in a PE chamber with a model leaf was cooled to a greater extent than the air in a chamber without a model leaf, although the temperature of the model leaf surface was higher than that of the floor surface of the chamber without the model leaf.

In contrast, many studies of urban parks have focused on cold patches in green areas （*e.g.*, Jauregui, 1990–1991; Eliasson and Upmanis, 2000; Hamada and Ohta, 2010; Hamada *et al.*, 2013）. For example, Narita *et al.* （2004） observed the temperature of a vegetation complex that consisted of zones of trees and turf grass and concluded that the turf grass zone was the source of cooling in the park at night because the temperatures of the air and surface of

the turf grass zone were lower than those of the tree zone. With respect to heat exchange, however, such cold patches usually form in places more isolated from the surrounding warmer urban atmosphere, and hence they probably help to cool the urban atmosphere to only a small extent. The objectives of this study were to evaluate the convective heat exchange at the canopy surface during nocturnal radiative cooling and the effects of the canopy surface area on cooling the surrounding air.

The sensible heat flux density due to convection (hereafter convective heat flux density) at the canopy surface per unit ground area, H, is described by

$$H = g_c (T_{air} - T_{canopy}), \qquad (1)$$

where T_{air} is the air temperature, T_{canopy} is the canopy surface temperature, and g_c is the convective heat transfer conductance. Note that the density is expressed per unit ground area. According to Eq. 1, as the conductance, g_c, increases, the canopy surface temperature increases, because H is in balance with the net radiation loss from the canopy surface. An increase of the surface temperature causes an increase of radiation loss and a concomitant increase of the convective heat flux density.

To explain the effect of the canopy surface area on the heat exchange between the plant canopy and air, we may rewrite g_c as the product of the convective heat transfer coefficient at the canopy surface, $h_{c\text{-}canopy}$, and the leaf area index of the canopy, LAI, as follows:

$$g_c = 2h_{c\text{-}canopy} \cdot LAI, \qquad (2)$$

in which the constant 2 accounts for the two sides of the leaf surface, with the coefficient assumed to be identical on both sides. In Eq. 2 we assumed that the wind-induced heat transfer processes in canopy boundary was represented by a single coefficient $h_{c\text{-}canopy}$ and the coefficient did not depend on LAI.

Equation 2 shows that both the LAI and $h_{c\text{-}canopy}$ contribute to the increase in g_c and thus to the increase of the convective heat flux, which consequently enhances air cooling. Okada *et al.* (2014) showed that the convective heat flux inside the PE chamber increased when a leaf model was introduced in the chamber. In this paper, we introduced three models with different LAI and conducted physical model experiments using a PE chamber to experimentally evaluate the dependence of the heat exchange at the plant canopy surface on the LAI during nocturnal radiative cooling. We also examined the relationship between the heat exchange and the canopy surface area using simple heat balance equations.

2. Physical Model Experiments

The PE chamber was developed by Okada *et al.* (2014) to investigate heat-exchange processes at the surface of a body exposed to shortwave and/or longwave radiation. For a full description of the PE chamber system and performance, see Okada *et al.* (2014); a brief synopsis follows. The PE chamber is similar to a wind tunnel covered with a plastic panel that transmits shortwave radiation (*e.g.*, Hino and Kanda, 1989), but the measurement section (hereafter PE section) of the PE chamber is covered with 0.02-mm-thick PE film with a transmissivity of both shortwave
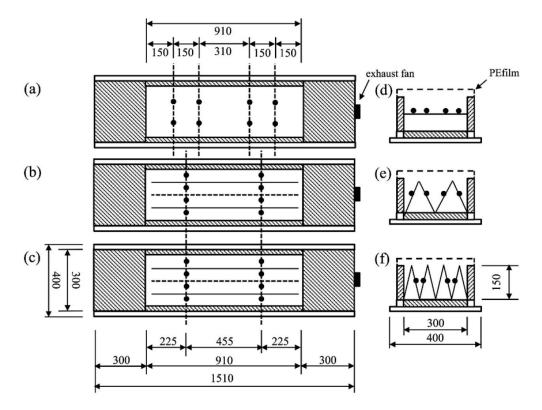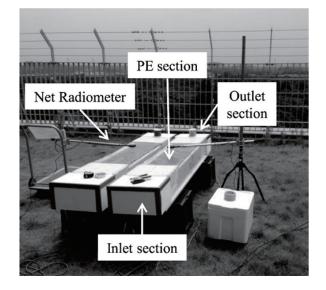

Fig. 1. A plane view (left) and a cross-section view (right) of the chamber with a leaf model for LAI = 1 (a, d), LAI = 2 (b, e), and LAI = 4 (c, f). Circles indicate the locations of temperature measurements on the model surface. Numbers are linear dimensions in mm.

and longwave radiation as large as 0.85. Therefore, the PE chamber allows model surfaces installed in the chamber to be exposed to radiation at levels similar to outdoor levels in the daytime as well as at night. The PE chamber was ventilated in the longitudinal direction by using an exhaust fan with an airflow speed of approximately 0.2 m s^{-1}. The use of the temperature difference between the air inlet and outlet and the other heat balance components of the PE chamber enabled us to evaluate the convective heat flux at the inside surface of the chamber.

Our interest lay in the dependence of the heat exchange at the canopy surface on the canopy surface area at night so that we did not take transpiration from leaves into consideration in this study. To simplify the heat exchange processes at the canopy surface, we introduced a single layer of the model canopy in the chamber so as to cover the entire surface of the floor of the PE section. In this way the radiative heat flux exchanged with the sky was intercepted by the canopy surface. To increase the LAI of the model canopy, we created inverted V-shape models, because the space for installing the model canopy was limited in the PE chamber. To vary the size of the canopy surface area, we prepared three models: one flat plane model and two inverted V-shape models. The models had surface areas equal to one, two, and four times the floor area. In other words, the model surface areas were equivalent to LAIs of 1, 2, and 4. The models for LAI = 1 were made from two single sheets of black Kent paper, each being 450 mm in length and 300 mm in width, and suspended at a height of 75 mm above the floor using thin wire （φ = 1.0 mm）parallel to the floor surface （Fig. 1a）. The models for LAI = 2 were made from four inverted V-shape sheets of black Kent paper, each being 450 mm in length, and folded in a triangular shape with a base width of 150 mm and a ridge height of 130 mm （Fig. 1b）. The models for LAI = 4 were made from eight sheets of black Kent paper, each being 450 mm in length and folded in a triangular shape, with a base width of 75 mm and a ridge height of 145 mm （Fig. 1c）.

Two PE chambers were placed on the roof of the Graduate

Fig. 2. Installation of two sets of the PE chambers placed on the grass-covered rooftop of the Graduate School of Life and Environment Sciences building.

School of Life and Environment Sciences building, University of Tsukuba, Tsukuba, Japan （36.87°N, 141.7°E）（Fig. 2）. Each chamber contained a different size of the model canopy inside. We conducted three experiments: a comparison of LAIs of 1 and 2 （hereafter LAI 1-2）, LAIs of 1 and 4 （hereafter LAI 1-4）, and LAIs of 2 and 4 （hereafter LAI 2-4）. The experiments were conducted during a clear night; for LAI 1-4 from 20:10 to 20:25 JST on 15 August 2013, for LAI 2-4 from 19:00 to 19:15 JST and for LAI 1-2 from 19:40 to 19:55 JST on 27 September 2013.

Copper-constantan thermocouples were used to measure the temperatures of the model canopy surface （Fig. 1）. The air and wall surface temperatures, which were needed to calculate the heat balance components of the PE chamber, were measured by thermocouples as described by Okada *et al.* （2014）. All of the thermocouples were connected to one common reference junction so as to minimize the errors in measurement of temperature difference between a pair of sensing thermocouples （Okada, 2010）. The resolution of the temperature difference measurement estimated from the datalogger resolution was an order of 0.01℃. The net longwave radiation above the PE section of the chamber was measured with a net radiometer （Q7, Radiation and Energy Balance Systems, Inc., Seattle, United States）. All the sensor signals as well as the reference temperatures of the thermocouples were collected by using a datalogger （CR-1000, Campbell Scientific, Logan, United States）with a sampling interval of 1 s and an averaging interval of 1 min for recording data. All data averaged over a 15-min sampling period were used for the analysis.

Okada *et al.* （2014）have proposed two ways to calculate the convective heat flux from a model surface installed in a PE chamber. The first approach is based on the heat balance of the PE chamber, and the second is based on the radiation balance at the surface. We applied the first approach, which is unique to the PE chamber technique, because it does not require the estimation of the radiation flux at the surface. The Appendix provides a detailed description of the equations used to calculate the heat balance components of the PE chamber.

3. Results of experiments

The 15-min average values of the air temperatures, surface temperatures, and temperature differences observed in the experiments are listed in Table 1. Each of the three experiments compared two different LAI models. The model surface temperature, T_m, was higher for the larger LAI model than for the smaller one in every experiment. In contrast, the outlet air temperature, T_{out}, was smaller for the larger LAI models, whereas the inlet air temperature, T_{in}, was the same between the two chambers. Consequently, the temperature difference between the model surface and the air decreased as the LAI increased.

In the LAI 1-2 and LAI 1-4 experiments, the temperature difference between the inlet and outlet air of the chamber, ΔT_a, was larger by about 0.2℃ in the cases of the LAI = 4 and 2 models when compared to the ΔT_a of the respective companion LAI = 1 model, whereas the ΔT_a was nearly the same for the LAI = 4 and 2 models in the LAI 2-4 experiment. Okada *et al.* （2014）reported similar results: ΔT_a was larger by 0.4℃ with the LAI = 2 model than without the model （LAI = 0）. Thus ΔT_a increases as the LAI increases, but it tends to approach an asymptotic value.

Table 1. Comparison of the air temperatures, surface temperatures, and the temperature differences in the chamber at night. The letters A and B in parentheses in the LAI row identify which one of the two chambers was used in the measurements.

Date	27 September		15 August		27 September	
LAI	2 (A)	1 (B)	4 (A)	1 (B)	4 (B)	2 (A)
T_m	12.5	12.2	27.5	25.8	14.6	13.0
ΔT_a	−1.0	−0.8	−0.9	−0.7	−1.0	−1.0
T_{out}	14.9	15.2	27.6	27.8	15.4	15.3
T_{in}	15.9	16.0	28.5	28.5	16.4	16.3
T_f	13.8	13.9	27.8	27.0	15.2	14.4
ΔT_w	−0.4	−0.8	0.1	−0.4	−0.6	−0.4
ΔT_f	−2.6	−2.2	−0.6	−1.0	−1.4	−2.4

Table 2 shows the heat balance components and the net longwave radiation below the PE film of the PE chambers calculated from the equations in the Appendix together with the net longwave radiation above the PE film of the chamber measured with the net radiometer.

The magnitude of the convective heat flux at the model surface, Q_{c-m}, and that of the net longwave radiation exchange at the upper and lower surface of the model, $R_{n-m} - R_{n-f}$, should be equivalent if radiation loss and sensible heat gain due to convection from the air were balanced at the model surface (Okada *et al.* 2014). The magnitude of those variables was similar but $R_{n-m} - R_{n-f}$ was slightly larger than Q_{c-m} in most cases. The disagreement of those values may be attributed partially to the errors accumulated in calculation of the heat balance components. It may also be attributed to the occurrence of dew condensation on the model surface, because we found that the paper model was dry at the beginning of the experiment but wetted at the end.

In the LAI 1-2 and LAI 1-4 experiments, the net longwave radiation flux density above the PE film, L_{n-a}, was more negative with the LAI = 2 and 4 models than with the LAI = 1 model. The implication is that the radiative heat loss from the chamber was larger for the larger LAI, a natural consequence of the higher surface temperature of the larger LAI models. The difference of the observed surface temperatures between the models, however, did not exactly correspond to the difference of net longwave radiation. The explanation may be that the limited number of thermocouples in the experiments did not properly measure the temperature over the whole model surface.

Radiative heat loss is the force that drives heat exchange by convection between the inside surfaces and the internal air of the chamber. Hence an increase of the radiative loss of heat accelerates cooling of the internal air. In the LAI = 2 chamber, the sum of the convective heat fluxes at the floor surface and the model surface, $Q_{c-f} + Q_{c-m}$, was in fact 1.2 times the analogous flux for LAI = 1, and the air temperature at the chamber outlet was approximately 0.2℃ lower for LAI = 2 than for LAI = 1.

In contrast, in the LAI 2-4 experiment, both L_{n-a} and Q_{c-m} in the chamber did not differ significantly between LAI = 2 and 4. As a

Table 2. Comparison of the heat balance components in the chamber. The letters A and B in parentheses in the LAI row identify which one of two chambers was used in the measurement. Asterisks denote the values measured with a net radiometer.

Date	27 September		15 August		27 September	
LAI	2 (A)	1 (B)	4 (A)	1 (B)	4 (B)	2 (A)
L_{n-a} (W m^{-2})	−45.5*	−41.2*	−37.1*	−30.6*	−47.9*	−47.9*
L_{n-b} (W m^{-2})	−41.9	−37.5	−34.7	−27.7	−44.8	−44.0
Q_{c-m} (W)	−9.4	−6.9	−6.9	−5.5	−10.1	−8.9
Q_{c-m}/A_f (W m^{-2})	−34.4	−25.3	−25.3	−20.1	−37.0	−32.6
$(Q_{c-m}/A_f)/L_{n-b}$	0.82	0.67	0.73	0.73	0.83	0.74
Q_{c-f} (W)	−1.1	−1.7	−1.3	−2.1	−0.6	−1.1
Q_v (W)	−9.3	−7.4	−7.5	−6.7	−9.4	−8.9
Q_p (W)	−0.9	−0.7	−0.8	−0.7	−0.9	−0.9
Q_{g-w} (W)	−0.2	−0.4	0.0	−0.2	−0.3	−0.2
Q_{g-f} (W)	−0.9	−0.8	−0.2	−0.4	−0.5	−0.9
R_{n-m} (W)	−11.4	−10.2	−9.5	−7.6	−12.2	−12.0
R_{n-f} (W)	−2.0	−2.5	−1.5	−2.5	−1.1	−2.0
$R_{n-m} - R_{n-f}$ (W)	−9.4	−7.7	−8.0	−5.1	−11.1	−10.0

result, the temperature differences between the air inlet and outlet of the chamber, ΔT_a, were identical (Table 1). Similar to the ΔT_a results, the convective heat exchange at the model surface and its resultant effect on air-cooling increased as the LAI increased, but it tended to approach an asymptotic value.

4. Heat balance analysis

The foregoing experimental results show that the effect of the canopy on air-cooling approaches an asymptotic value as the canopy surface area becomes large. In the following paragraphs, we try to evaluate the relationship between the canopy effect on air-cooling and the canopy surface area (LAI) by using simple heat balance equations.

To simulate the PE chamber, we assumed a segment of an air layer in which a single-layer canopy model was suspended. We also assumed that the movement of air in the air layer was unidirectional from one end of the segment to the other, and we assumed that there was no convective heat transfer from the air layer to the adjacent upper or lower air layers (Fig. 3). This one-dimensional airflow is consistent with the ventilation of the air in the PE chamber and thus creates a temperature difference between the inlet and the outlet of the segment. The convective heat exchange between the air and the canopy surface is balanced by the heat transported by the airflow as follows:

$$g_c(T_{air} - T_{canopy}) = g_v(T_{in} - T_{out}), \qquad (3)$$

where T_{in} and T_{out} are the incoming and outgoing air temperatures of the segment of the air layer, respectively. The parameter g_c is the convective heat transfer conductance defined by Eq. 2. The parameter g_v is the heat transfer conductance due to airflow and is equal to the product of the heat capacity and the airflow rate per unit area (Eq. 4); g_v may likewise be defined as the heat transfer conductance due to ventilation of the PE chamber as follows:

$$g_v = \rho c_p V / A_f. \qquad (4)$$

where ρ is the air density, c_p is the specific heat of air at constant pressure, V is the airflow rate and A_f is the floor surface area.

When no latent heat transfer is assumed at night, the surface temperature of the canopy depends primarily on convective heat exchange with the air and longwave radiation exchange with the sky and with the ground surface beneath the canopy. The experimental results in Table 2 showed that the radiative heat exchange between the model surface and the floor surface, R_{n-f}, was small and less variable compared to the analogous exchange between the model surface and the sky, R_{n-m}. In order to solve the equations arithmetically we therefore neglected the radiation exchange with the ground surface beneath the canopy and expressed the heat balance at the canopy surface as

$$g_c(T_{air} - T_{canopy}) = g_r(T_{canopy} - T_{sky}). \qquad (5)$$

where T_{sky} is the sky temperature, and g_r is the radiative heat transfer conductance. Although the linear approximation of radiation exchange in Eq. 5 combined with Eq. 6 leads to an error of 5% in calculation of radiation exchange for the temperature difference ($T_{canopy} - T_{sky}$) of 10℃, we introduced a linear-form equation to solve the equations arithmetically. The radiative heat transfer conductance, g_r, is conventionally approximated by the first term of the Taylor series expansion of the radiation exchange equation as follows:

$$\begin{aligned} g_r &= 4\sigma(T_{sky} + 273.15)^3, \quad \text{for } LAI \geq 1 \\ g_r &= 4\sigma(T_{sky} + 273.15)^3 \cdot \text{LAI, for } LAI < 1, \end{aligned} \qquad (6)$$

where σ is Stefan-Boltzmann constant ($= 5.67 \times 10^{-8}$ W m^{-2} K^{-4}). We assumed that the ground surface was entirely covered by the canopy when LAI was larger than one. In this case, the radiative heat flux exchanged with the sky is intercepted by the area equivalent to the ground area regardless of the magnitude of LAI. In other words, for heat flux calculation on a ground area basis the view factor of the canopy cover area to the sky is equal to one. This is the reason why the first equation in Eq. 6 does not relate to LAI. We also assumed a large single leaf suspended horizontally in the air layer when LAI was smaller than one. In this case, the sky view factor of the canopy is equal to one, but the radiation is intercepted by the leaf surface area, hence LAI. This is the reason why the second equation in Eq. 6 relates directly to LAI.

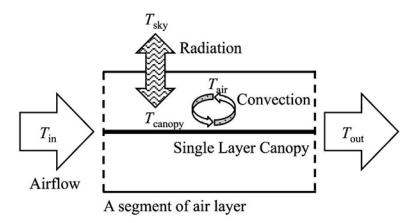Equations 3 and 5 lead to the following heat balance equation

Fig. 3. Illustration of a simple heat balance model for a segment of the air layer and a single-layer canopy surface. Refer to the text for the variables in the figure.

for airflow, convection and radiation:

$$g_v(T_{in} - T_{out}) = g_c(T_{air} - T_{canopy}) = g_r(T_{canopy} - T_{sky}). \quad (7)$$

We assumed that the air temperature in the air layer changed linearly from the inlet to the outlet. Therefore, $T_{air} = (T_{in} + T_{out}) / 2$. We obtained the canopy surface temperature by rearranging the first two terms in Eq. 7:

$$T_{canopy} = \frac{(g_c - 2g_v)T_{in} + (g_c + 2g_v)T_{out}}{2g_c}. \quad (8)$$

From the airflow and radiative components of Eq. 7, we also obtained the canopy surface temperature as follows:

$$T_{canopy} = \frac{g_v(T_{in} - T_{out}) + g_r T_{sky}}{g_r}. \quad (9)$$

The outgoing air temperature of the air layer was obtained by substituting Eq. 9 into Eq. 8:

$$T_{out} = \frac{(2g_v g_c - g_c g_r + 2g_v g_r)T_{in} + 2g_c g_r T_{sky}}{2g_v g_c + g_c g_r + 2g_v g_r}$$
$$= \frac{(2g_v - g_r + 2g_v g_r/g_c)T_{in} + 2g_r T_{sky}}{2g_v + g_r + 2g_v g_r/g_c} \quad (10)$$

Similarly, the outgoing air temperature was obtained from the airflow and convective components of Eq. 7:

$$T_{out} = \frac{(2g_v - g_c)T_{in} + 2g_c T_{canopy}}{2g_v + g_c}. \quad (11)$$

From the radiative and airflow components of Eq. 7, the outgoing air temperature was also obtained as follows:

$$T_{out} = \frac{g_v T_{in} + g_r(T_{sky} - T_{canopy})}{g_v}. \quad (12)$$

The canopy surface temperature was thus obtained by substituting Eq. 12 into Eq. 11:

$$T_{canopy} = \frac{2g_v g_c T_{in} + (2g_v g_r + g_c g_r)T_{sky}}{2g_v g_c + g_c g_r + 2g_v g_r}$$
$$= \frac{2g_v T_{in} + (2g_v g_r/g_c + g_r)T_{sky}}{2g_v + g_r + 2g_v g_r/g_c}. \quad (13)$$

Equations 10 and 13 indicate that both the outgoing air temperature and the canopy surface temperature usually lie midway between the sky temperature and the incoming air temperature. As the convective heat transfer conductance, g_c, increases, the canopy surface temperature approaches the incoming air temperature, while the outgoing air temperature approaches the sky temperature. With an infinitely large g_c, the outgoing air temperature and the canopy surface temperature converge to the values determined by Eqs. 14 and 15, respectively:

$$T_{out} = \frac{(2g_v - g_r)T_{in} + 2g_r T_{sky}}{2g_v + g_r}. \quad (14)$$

$$T_{canopy} = \frac{2g_v T_{in} + g_r T_{sky}}{2g_v + g_r}. \quad (15)$$

Equations 10 and 13 clearly show that a large g_c resulting from a large LAI raises the canopy surface temperature but lowers the outgoing air temperature, and both temperatures approach their respective asymptotic values.

From Eqs. 10 and 13, we calculated the dependence of the air-cooling effect on the LAI by using the data from the experiment on 27 September 2013, namely the air temperature of 16.3℃ and the apparent sky temperature of 4.3℃ estimated from the downward longwave radiation below the PE film, with the sky assumed to be a black body. In the experiments on 27 September, the convective heat transfer coefficients at the canopy surface, $h_{c\text{-canopy}}$, ranged from 3.3 W m^{-2} ℃$^{-1}$ (LAI = 2) to 3.7 W m^{-2} ℃$^{-1}$ (LAI = 4). We therefore used the average value 3.5 W m^{-2} ℃$^{-1}$ for $h_{c\text{-canopy}}$ in Eq. 2. For the heat transfer conductance due to airflow, g_v, we used the same value as the conductance due to ventilation used in the PE chamber experiment; 33.2 W m^{-2} ℃$^{-1}$.

In the heat balance equations, the net longwave radiation flux above the canopy surface is balanced with the convective heat
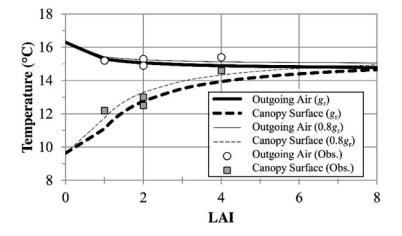

Fig. 4. Dependence of the outgoing air temperature and canopy surface temperature on the LAI. Thick lines were calculated using g_r defined by Eq. 6 and thin lines using 0.8 g_r to compare with the observed temperatures indicated by the symbols.
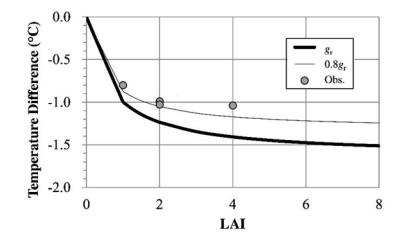
Fig. 5. Dependence of the temperature difference between the incoming and outgoing air on the LAI. See Fig. 4 for a description of the lines.

transfer flux, because we did not take the radiation exchange with the ground surface below the canopy into consideration. As shown in Table 2, however, the net longwave radiation flux above the canopy, R_{n-m} $(=A_f L_{n-b})$, is not equivalent to the convective heat transfer flux, Q_{c-m}, in the experiment. To compare the temperatures calculated from the heat balance equations with those observed in the experiment, we tried to simulate the experimental conditions by multiplying the radiative heat conductance, g_r by the ratio, $(Q_{c-m} / A_f) / L_{n-b}$. The thick lines in Figs. 4 and 5 were calculated with g_r multiplied by one, and the thin lines with g_r multiplied by 0.8 obtained from the experiments on 27 September. The thin lines show agreement between the calculated and observed temperatures.

As a function of LAI, the outgoing air temperature and the canopy surface temperature decreased and increased, respectively, in a nonlinear manner（Fig. 4）. Both temperatures closely approached their respective asymptotic values. In contrast, the temperature difference between the incoming and outgoing air decreased as the LAI increased, and it approached an asymptotic value of approximately −1.5℃（Fig. 5）. Figure 4 indicates that cooling of the air traveling through the canopy increased at night as the LAI increased, whereas the canopy surface temperature increased. Figure 5 indicates that the effect of the canopy on air-cooling increased as the LAI increased, but the cooling approached a maximum value only at a very large LAI.

This heat balance analysis simulates the nonlinear responses of the canopy surface temperature and the changes of the temperature of the air traveling through the canopy as functions of the LAI. The results calculated from the equations show relative trends similar to those observed in the experiments. This suggests that the asymptotic behavior of air cooling is resulted from the different responses of convection and radiation to LAI, i.e. the convective heat flux per unit ground area depends on LAI but the radiative flux does not.

5. Conclusion

In this study, we investigated the relationship between the LAI and its effect on air-cooling during nocturnal radiative cooling.

We hypothesized that the enhancement of air-cooling was greater when the LAI of a plant canopy was larger.

In the model experiments, the radiation losses from the experimental chamber increased as the LAI of the model canopy increased. Larger radiation losses resulted from higher surface temperatures that were caused by enhanced heat convection due to increased LAIs. The enhanced heat convection led to accelerated air-cooling, although the canopy surface temperature was relatively high. The experimental results revealed the effects of the canopy surface area on heat exchange processes and resultant air-cooling, but the response of the canopy surface and/or air temperatures seemed to be nonlinear functions of the LAI and tended to converge to asymptotic value as the LAI increased.

To elucidate the relationship between the canopy surface temperatures or air temperatures and the LAI, we introduced simple heat balance equations that described the heat exchanges of a single-layer canopy model exposed to radiative cooling at night. These equations simulated the heat fluxes associated with a leaf model suspended in the PE chamber. Numerical simulations using these equations clearly revealed that as the LAI increased, the canopy surface temperature increased, but the temperature of the air traveling through the canopy decreased. Both temperatures gradually approached asymptotic values. The effects of the LAI on these temperatures were due primarily to changes in convective heat transfer conductance at the canopy surface, as shown in Eq. 2. Air-cooling may therefore be accelerated by high wind speeds and/or by vegetation with small leaves, because the convective heat transfer conductance varies according to the factors that affect the convective heat transfer coefficient, such as wind speed and/or the size of leaves.

Although the study described here was limited physically in terms of size and wind regime, both the experimental and numerical results suggest that air-cooling is accelerated more as the LAI increases, whereas the canopy surface temperature becomes higher as the LAI increases. These results also suggest that warmer vegetation, such as tall trees compared to short grasses, should be given consideration as a means of cooling urban air in a green park at night.

Appendix

List of symbols

A_f Area of the floor surface（m²）

A_p Area of the polyethylene film surface（m²）

A_w Surface Area of the sidewalls（m²）

c_p Specific heat of air at constant pressure（J K⁻¹ kg⁻¹）

d Thickness of extruded polystyrene foam panel（= 0.03 m）

g_c Convective heat transfer conductance（W m⁻² ℃⁻¹）

g_r Radiative heat transfer conductance（W m⁻² ℃⁻¹）

g_v Ventilation heat transfer conductance（W m⁻² ℃⁻¹）

$h_{c\text{-}canopy}$ Convective heat transfer coefficient at the canopy surface（W m⁻² ℃⁻¹）

h_t Heat transmission coefficient（W m⁻² ℃⁻¹）

H Convective heat flux density at the canopy surface（W m⁻²）

$L_{n\text{-}a}$ Net longwave radiation flux density above the polyethylene film（W m⁻²）

$L_{n\text{-}b}$ Net longwave radiation flux density below the polyethylene film（W m⁻²）

LAI Leaf area index

$Q_{c\text{-}f}$ Convective heat flux at the floor surface（W）

$Q_{c\text{-}m}$ Convective heat flux at the leaf model surface（W）

$Q_{g\text{-}f}$ Conductive heat flux through the floor（W）

$Q_{g\text{-}w}$ Conductive heat flux through the sidewall（W）

Q_p Heat transmission flux through the polyethylene film（W）

Q_v Heat flux due to ventilation（W）

r_m Reflectivity of the leaf model surface for longwave radiation（= 0.11）

r_p Reflectivity of the polyethylene film for longwave radiation（= 0.11）

$R_{n\text{-}f}$ Net longwave radiation flux at the floor surface（W）

$R_{n\text{-}m}$ Net longwave radiation flux at the upper surface of the leaf model（W）

t_p Transmissivity of the polyethylene film for longwave radiation（= 0.85）

T_{air} Air temperature near the canopy（℃）

T_{canopy} Canopy surface temperature（℃）

T_f Floor surface temperature（℃）

T_{in} Air temperature at the air inlet of the polyethylene chamber or incoming air temperature of the segment of an air layer（℃）

T_{inside} Air temperature inside the polyethylene chamber（℃）

T_m Leaf model surface temperature（℃）

T_{out} Air temperature at the air outlet of the polyethylene chamber or outgoing air temperature of the segment of an air layer（℃）

$T_{outside}$ Air temperature outside the polyethylene chamber（℃）

T_{sky} Sky temperature（℃）

V Ventilation rate of the exhaust fan or airflow rate in the segment of an air layer（= 0.0075 m³ s⁻¹）

ε_f Emissivity of the floor surface（= 0.89）

ε_m Emissivity of the leaf model surface（= 0.89）

ε_p Emissivity of the polyethylene film（= 0.04）

λ Heat conductivity of the extruded polystyrene foam（= 0.04 W m⁻¹ K⁻¹）

ρ Air density（kg m⁻³）

σ Stefan-Boltzmann constant（= 5.67×10⁻⁸ W m⁻² K⁻⁴）

ΔT_a Air temperature difference between the inlet and the outlet of the polyethylene chamber（outlet − inlet）（℃）

ΔT_f Temperature difference between the inside and the outside surface of the floor（inside − outside）（℃）

ΔT_w Temperature difference between the inside and the outside surface of the sidewall（inside − outside）（℃）

Calculation of the net radiation fluxes and the heat balance components

The net longwave radiation flux density below the PE film, $L_{n\text{-}b}$, is calculated from the following equations derived from the radiation balance of the PE chamber with a measured value for the net longwave radiation flux density above the PE film, $L_{n\text{-}a}$ and the model leaf temperature, T_m and an estimate for the PE film temperature, T_p（Okada *et al.*, 2014）.

$$L_{n\text{-}b} = \frac{1 - r_m}{1 - r_m r_p}(\varepsilon_p \sigma T_p^4 + t_p L_{sky}) + \frac{r_p - 1}{1 - r_m r_p}\varepsilon_m \sigma T_m^4 \qquad (A1)$$

The downward longwave radiation from the sky, L_{sky}, is given by,

$$L_{sky} = \frac{(1 - r_m r_p)L_{n\text{-}a} + (1 - r_m r_p + t_p r_m)\varepsilon_p \sigma T_p^4 + t_p \varepsilon_m \sigma T_m^4}{(1 - r_p)(1 - r_m r_p) - t_p^2 r_m}. \quad (A2)$$

The net longwave radiation flux at the upper leaf model surface, $R_{n\text{-}m}$, is equal to that below the PE film, hence,

$$R_{n-m} = A_f L_{n-b}. \qquad (A3)$$

The net longwave radiation flux at the floor surface, $R_{n\text{-}f}$, is calculated from the leaf model and the floor surface temperatures assuming the two surfaces in parallel as follows:

$$R_{n-f} = \frac{1}{1/\varepsilon_f + 1/\varepsilon_m - 1}\sigma(T_m^4 - T_f^4). \qquad (A4)$$

The heat transfer due to ventilation, Q_v, is calculated by using the air temperature difference between the inlet and the outlet of the chamber, ΔT_a, and the ventilation rate, V, as follows:

$$Q_v = \rho c_p V \Delta T_a. \qquad (A5)$$

The heat transmission through the PE film, Q_p, is estimated from the difference between the inside and outside air temperatures and the heat transmission coefficient, h_t, as follows:

$$Q_p = A_p h_t (T_{inside} - T_{outside}). \qquad (A6)$$

The conductive heat components, $Q_{g\text{-}w}$ and $Q_{g\text{-}f}$, are calculated from the temperature difference between the inside and the outside surface of the sidewall, ΔT_w, or of the floor panel, ΔT_f, the heat conductivity, λ, and the thickness, d, of the extruded polystyrene foam panel as follows:

$$Q_{g-w} = A_w \frac{\lambda}{d} \Delta T_w \tag{A7}$$

$$Q_{g-f} = A_f \frac{\lambda}{d} \Delta T_f. \tag{A8}$$

The convective heat flux at the leaf model surface, Q_{c-m}, is calculated from the heat balance equation（Okada *et al*., 2014），

$$Q_{c-m} = Q_v + Q_p + Q_{g-w} - Q_{c-f}. \tag{A9}$$

The convective heat flux at the floor, Q_{c-f}, is calculated from the heat balance at the floor surface,

$$Q_{c-f} = R_{n-f} - Q_{g-f}. \tag{A10}$$

References

Eliasson, I., and Upmains, H., 2000: Nocturnal airflow from urban parks-implications. *Theoretical and Applied Climatology*, **66**（1–2），95–107.

Hamada, S., and Ohta, T., 2010: Seasonal variations in the cooling effect of urban green areas on surrounding urban areas. *Urban Forestry & Urban Greening*, **9**, 15–24.

Hamada, S., Tanaka, T., and Ohta, T., 2013: Impacts of land use and topography on the cooling effect of green areas on surrounding urban areas. *Urban Forestry & Urban Greening*, **12**, 426–434.

Hino, M., and Kanda, M., 1989: Study on the climate moderation effect of plant by lysimeter with wind-tunnel. *Journal of Japan Society of Hydrology and Water Resources*, **2**（1），61–69.（in Japanese with English abstract）

Honjo, T., and Takakura, T., 2000a: Validation of the two dimensional k-ε model for analysis of the thermal effect of urban green areas. *Journal of Agricultural Meteorology*, **56**（4），243–251.（in Japanese with English abstract）

Honjo, T., and Takakura, T., 2000b: Simulation of the influence of urban green areas with various scales and allocation. *Journal of Agricultural Meteorology*, **56**（4），253–260.（in Japanese with English abstract）

Huang, H. Y., Margulis, S. A., Chuand, C. R., and Tsai, H. C., 2011: Investigation of the impacts of vegetation distribution and evaporative cooling on synthetic urban daytime climate using a coupled LES-LSM model. *Hydrological Processes*, **25**（10），1574–1586.

Jauregui, E., 1990–1991: Influence of a large urban park on temperature and convective precipitation in a tropical city. *Energy and Buildings,* **15**（3–4），457–463.

Kanda, M., and Hino, M., 1990a: Numerical simulation of soil-plant-air system（1）modeling of plant system. *Journal of Japan Society of Hydrology and Water Resources*, **3**（3），37–46.（in Japanese with English abstract）

Kanda, M., and Hino, M., 1990b: Numerical simulation of soil-plant-air system（2）numerical experiment on the effect of plant on meteorological and environment. *Journal of Japan Society of Hydrology and Water Resources*, **3**（3），47–55.（in Japanese with English abstract）

Narita, K., Mikami, T., Sugawara, H., Honjo, T., Kimura, and K., Kuwata, N., 2004: Cool-island and cold air-seeping phenomena in an urban park, Shinjuku-Gyoen, Tokyo. *Geographical Review of Japan*, **77**（6），403–420.（in Japanese with English summary）

Okada, M., 2010: How to measure temperature accurately（3）A use of thermocouples. *Climate in Biosphere*, **10**, A-4.（in Japanese）

Okada. M., Okada, M., and Kusaka, H., 2014: A polyethylene chamber for use in physical modelling of heat exchange on surfaces exposed to a radiation regime. *Boundary-Layer Meteorology*, **153**（2），305–325.